Microstructure Evolution and Hardness of an Ultra-High Strength Cu-Ni-Si Alloy During Thermo-mechanical Processing

Q. Lei, Z. Li, W.P. Hu, Y. Liu, C.L. Meng, B. Derby, and W. Zhang

Microstructure evolution and hardness changes of an ultra-high strength Cu-Ni-Si alloy during thermo-mechanical processing have been investigated. For hot-compressive deformation specimens, dynamic recrystallization preferentially appeared on deformation bands. As deformation temperature increased from 750 to 900 °C, elongated grains with the Cubic texture {001} ⟨100⟩ were substituted by recrystallized grains with Copper texture {112} ⟨111⟩. For the samples having undergone cold rolling followed by annealing, static recrystallization preferentially occurred in the deformation bands, and then complete recrystallization occurred. Goss, Cubic, and Brass textures remained after annealing at 600 and 700 °C for 1 h; R texture {111} ⟨211⟩ and recrystallization texture {001} ⟨100⟩ were formed in samples annealed at 800 and 900 °C for 1 h, respectively. For samples processed under multi-directional forging at cryogenic temperature, the hardness was increased as a result of work hardening and grain refinement strengthening. These were attributed to the formation of equiaxed sub-grain structures and a high dislocation density.

1. Introduction

Copper and its alloys possess a wide range of properties that make them invaluable for many applications (Ref 1-4). The copper industry has invested much research effort over the years to create materials capable of meeting users' needs. In past decades, Cu-Be alloys have been used in a broad spectrum of applications spanning the automotive, aerospace, electronics, and medical industries. The toxicity of beryllium, however, and its poor anti-stress relaxation property, limit many modern applications (Ref 5, 6). An example being elastic conductive components, such as electrical contacts and, conductive blades and springs that are developing rapidly and they require higher performance than that provided by previously used Cu-Be alloys. To meet the requirement of the new devices, the materials must possess ultra-high strength (>1000 MPa), good conductivity ($>20\%$ IACS), and excellent anti-stress relaxation property ($R \leq 10\%$, at 150 °C). Several novel copper alloys, such as Cu-Ni-Sn (Ref 7), Cu-Ni-Zn (Ref 8), and Cu-Ni-Al

(Ref 9), have been studied over the past 40 years. These alloys exhibit ultra-high strength (>1000 MPa), but their electrical conductivities (below 15% IACS) are far lower than that of Cu-Be alloys (25% IACS). Cu-Ni-Si alloys stirred researchers' interest because of their high strength and good electrical conductivity (Ref 10-13). For example, Cu-Ni-Si alloys with high content of Ni and Si, were strengthened due to dispersed nano-scale particles formed during aging (Ref 14-19). Some Cu-Ni-Si alloys exhibit high strength, good electrical conductivity, and excellent anti-stress relaxation properties (Ref 20-22).

Previous investigations have focused on thermo-mechanical treatment, phase transformation, and precipitation behavior of the Cu-Ni-Si alloys. In fact, both dynamic recrystallization and static recrystallization play essential roles in achieving fine grains and uniform microstructures (Ref 23). To maximize the comprehensive performance, thermo-mechanical process should be studied systematically. Though there have been many investigations on the relationship between microstructure and mechanical properties in Cu-Ni-Si systems, most of these only focuses on the aging hardening behavior. In this study, we are trying to quantify and describe the effects of thermo-mechanical treatment on the hardness and microstructure evolution of a Cu-Ni-Si alloy in detail. Behavior of hot-compressive deformation (HCD), cold rolling deformation followed by annealing treatment (CRD + AT), and multi-directional forging (MDF) were investigated to optimize the thermo-mechanical treatment conditions and to develop better Cu-Ni-Si alloys.

Q. Lei, School of Materials Science and Engineering, Central South University, Changsha 410083, China and Department of Materials Science and Engineering, College of Engineering, University of Michigan, Ann Arbor 48109-2136; Z. Li, School of Materials Science and Engineering, Central South University, Changsha 410083, China; W.P. Hu, Institute of Physical Metallurgy and Metal Physics, RWTH Aachen University, 52056 Aachen, Germany; Y. Liu, C.L. Meng, and W. Zhang, State Key Laboratory of Powder Metallurgy, Changsha 410083, China; and B. Derby, Department of Materials Science and Engineering, College of Engineering, University of Michigan, Ann Arbor 48109-2136. Contact e-mail: lizhou6931@csu.edu.cn.

2. Experimental Procedures

The Cu-6.0Ni-1.0Si-0.5Al-0.15Mg-0.1Cr (wt.%) alloy ingots were processed in a medium frequency induction-melting furnace and then cast in a swage. After the surface defects were removed, 70 mm × 35 mm × 50 mm as-cast ingots were homogenized at 940 °C for 4 h. Four different process routes

Table 1 Process routes of thermo-mechanical treatments

Routes	Detailed process parameters	Characterization methods
HCD	Homogenization (940 °C/4 h), hot compression deformation (750, 800, 850, 900, and 900 °C by 60%)	Optical microscopy, electron back-scattered diffraction
CRD + AT	Homogenization(940 °C/4 h), hot rolled (by 80%, at 850 °C), solid solution treatment (980 °C/4 h), cold rolling deformation (by 50%), annealing (600, 700, 800, and 900 °C for 1 h)	Optical microscopy, orientation distribution function maps, transmission electronic microscopy, hardness measurements
MDF	Homogenization (940 °C/4 h), room-temperature multi-direction forging (RTMDF)/cryogenic temperature multi-direction forging (CTMDF), (1, 2, 4, and 8 cycles)	Optical microscopy, transmission electronic microscopy, hardness measurements
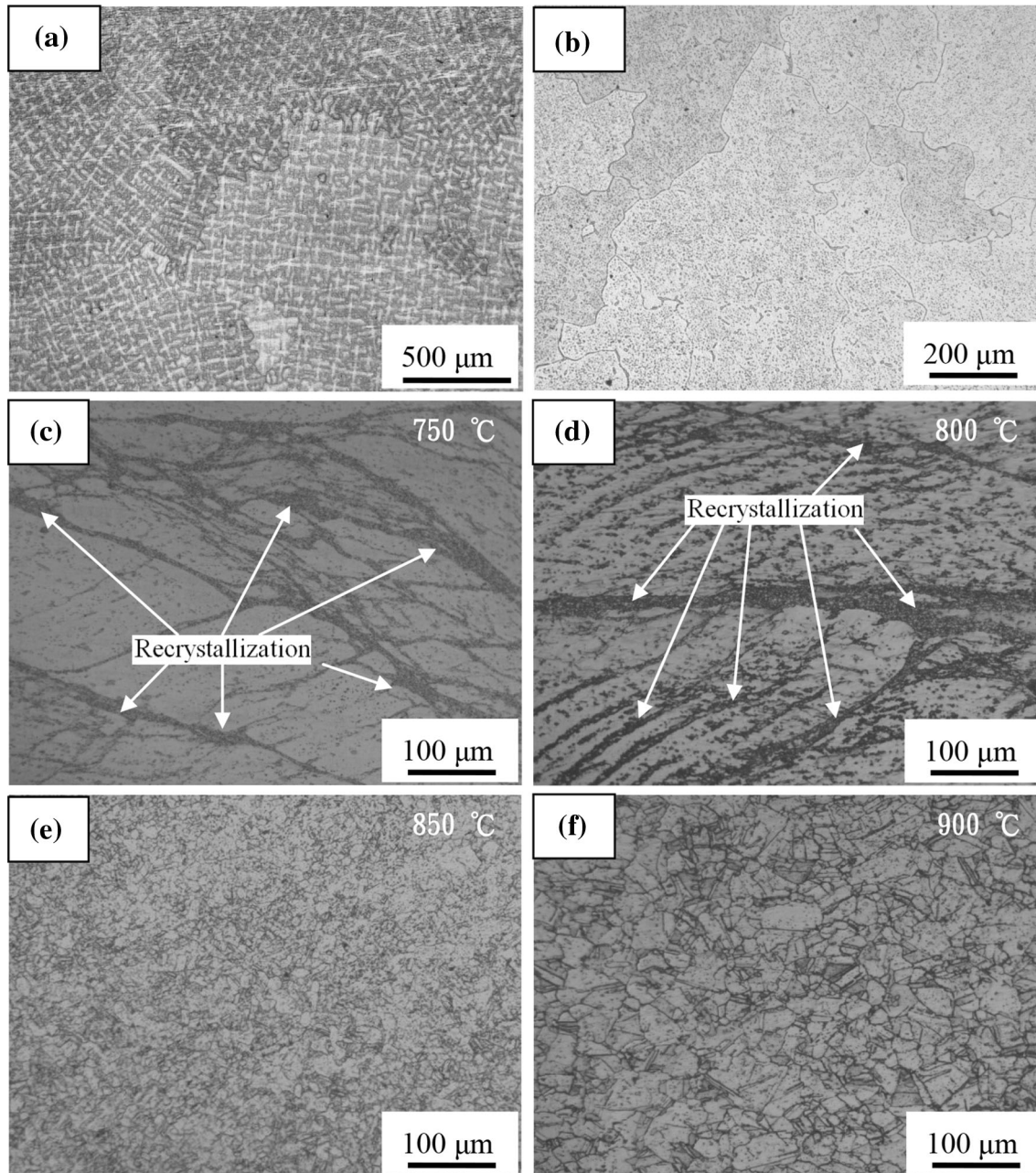
Fig. 1 Microstructure of specimens: (a) as-cast state; (b) homogenization at 940 °C for 4 h, and hot compression at different temperatures with strain rates of 0.001 s^{-1}; (c) 750 °C;(d) 800 °C; (e) 850 °C; (f) 900 °C
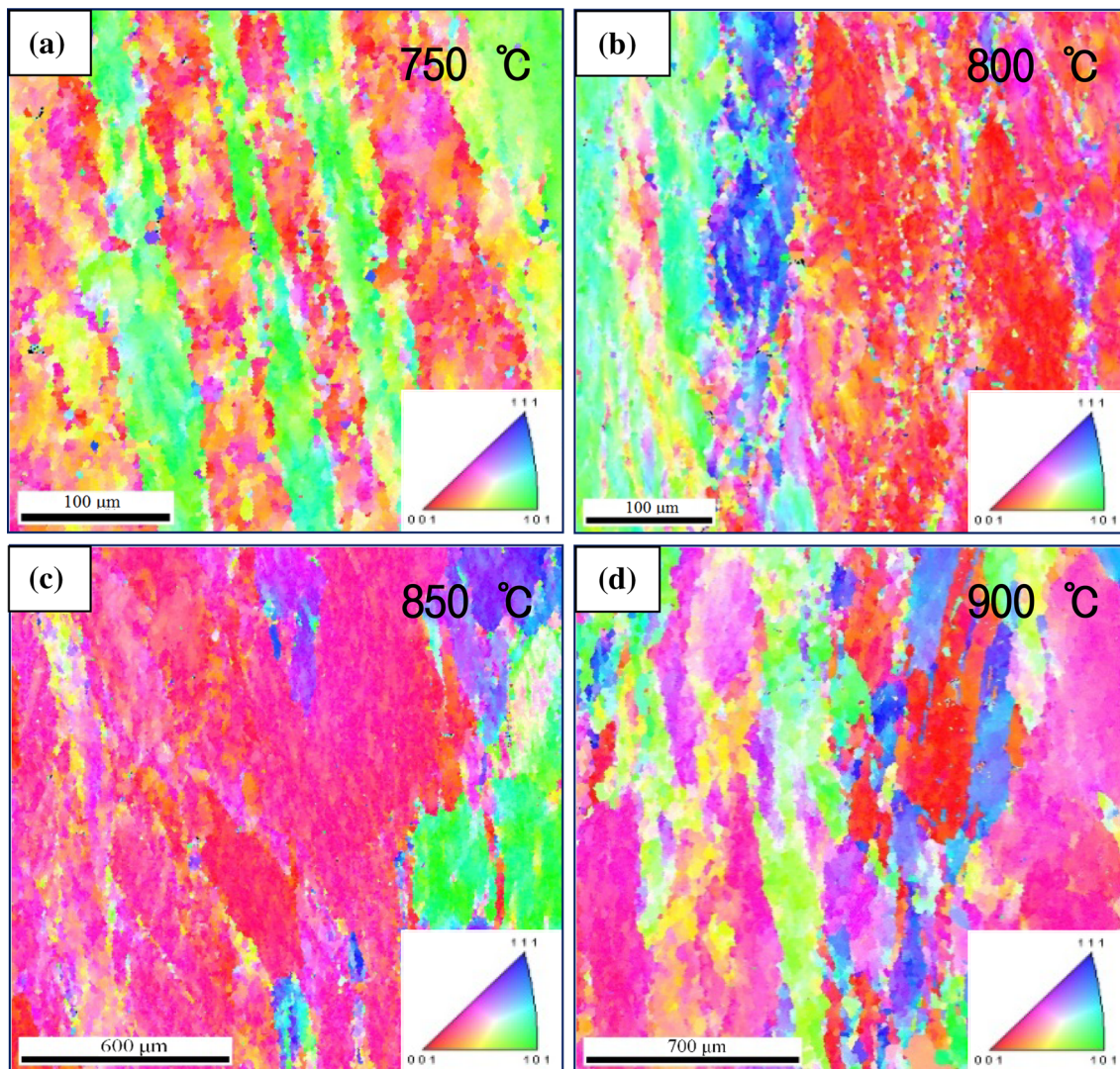
Fig. 2 EBSD micrographs showing the microstructure of specimen hot deformed by 60% at different temperatures with strain rate of 0.001 s^{-1}. (a) 750 °C; (b) 800 °C; (c) 850 °C (Ref 12); (d) 900 °C

were selected to study the microstructure evolution and hardness changes of the Cu-Ni-Si alloy during various thermo-mechanical treatments, all shown in Table 1. Hot compression deformation (HCD) specimens, with diameter of 10 mm and length of 15 mm, were cut from a homogenized ingot by electrical-discharge machining. The HCD experiments were conducted on a Gleeble-1500 thermo-mechanical simulator, with a strain rate of 0.001 s^{-1} and deformation temperatures of 750, 800, 850, and 900 °C. The heating rate was 5 °C/s. The specimens were warmed at deformation temperatures for 3 min. Then the specimens were compressively deformed by a total strain of 60% in an argon-protected atmosphere. Final thickness of the deformed samples was 6 mm. Cold rolling deformation (CRD) samples (50 mm × 30 mm × 10 mm) were cut from the homogenized ingots, then hot rolled by 80% at 850 °C, and the rolled samples (150 mm × 50 mm × 2 mm) were cut into three small sheets (50 mm × 50 mm × 2 mm), and solid solution was treated at 980 °C for 4 h. Then the super-saturated solid solution samples (50 mm × 50 mm × 2 mm) were cold rolled separately by 30, 50, and 80%, with final thickness of 1.4, 1, 0.4 mm, respectively. CRD + AT speci-mens (10 mm × 10 mm × 1 mm) were cut from the 50% cold-

rolled samples (90 mm × 55 mm × 1 mm), and then were annealed at 600, 700, 800, and 900 °C for 1 h.

The cubic multi-directional forging (MDF) specimens with dimensions of 15 mm × 15 mm × 15 mm were cut from the homogenized ingot (70 mm × 35 mm × 50 mm). The MDF samples were deformed using a cold-forging press with a strain rate of 10 s^{-1}. The direction of the samples was rotated every pass by an angle of 90°. Cryogenic temperature multi-directional forging (CTMDF) and room-temperature multi-directional forging (RTMDF) were carried out to investigate the microstructure evolution and hardness changes. All of the CTMDF samples were immersed in liquid nitrogen (−196 °C) for 10 min before each forging pass. Single strain was 0.2 after each pass. The cumulative strains after each cycle (1 cycle includes 3 passes) of MDF were 0.6. In the present study, both CTMDF and RTMDF were carried out to cumulative strains of 0.6, 1.2, 2.4, and 4.8 (i.e., 1, 2, 4, and 8 cycles).

Microstructures of specimens coming from HCD, CRD + AT, and CTMDF were observed using a Leica optical microscope. The macro-textures of CRD sheets were measured using an XRD texture device with orientation distribution functions (ODF). Micro-textures of HCD and CRD + AT
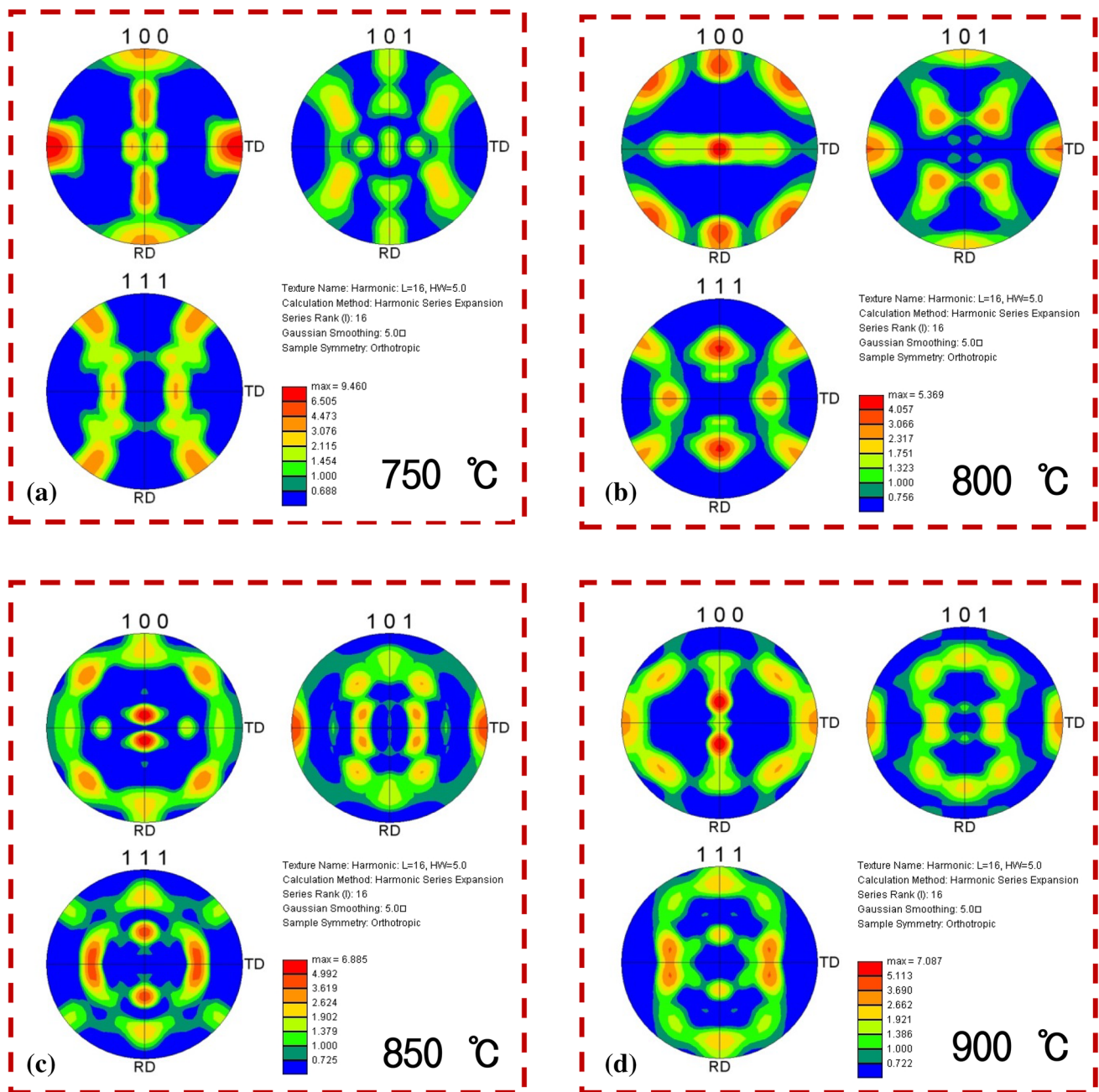
Fig. 3 Pole figure analysis of specimen after hot-compressive deformed by 60% at different temperatures. (a) 750 °C; (b) 800 °C; (c) 850 °C (Ref 12); (d) 900 °C

specimens were measured using a Siron 200 scanning electron microscope (FEI Co., Holland) with an electron back-scatter diffraction (EBSD) detector. A JEOL JEM 2000F transmission electron microscope was used to observe the microstructure of the CRD + AT and CTMDF specimens.

3. Results and Discussion

3.1 Microstructure of Hot Deformation Samples

Figure 1 shows the microstructures of specimens in the as-cast state, homogenization at 940 °C for 4 h, and hot com-pression at different temperatures with strain rates of 0.001 s⁻¹. Dendritic grains are observed in Fig. 1a, which were attributed to the non-equilibrium solidification process. Thus, a homog-enization treatment is required for uniform structure. After homogenization at 940 °C for 4 h, dendritic structures were eliminated (Fig. 1b) (Ref 22). Figure 1c-f show the microstruc-ture evolution of the HCD specimens. Partial dynamic recrys-tallization occurred in the deformation bands as the specimen was deformed at 750 °C (Fig. 1c). Increasing the deformation temperature to 800 °C, fine recrystallized grains appeared inside the grains as well as the deformation bands (Fig. 1d). Further increasing the deformation temperature to 850 °C, fine recrystallization grains appeared in the whole sample (Fig. 1e).
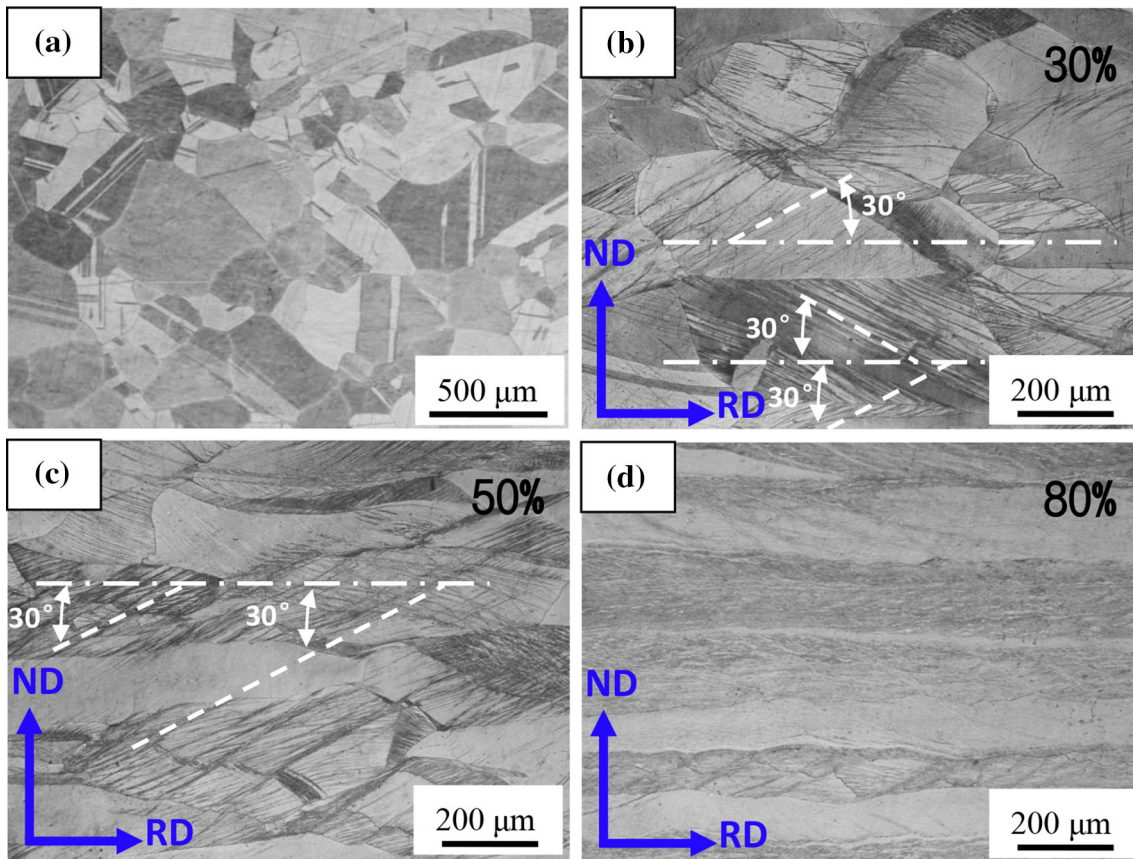
Fig. 4 Microstructure of sample sheets with different cold rolling deformation. (a) Super-saturated solid solution; (b) 30%; (c) 50%; (d) 80%
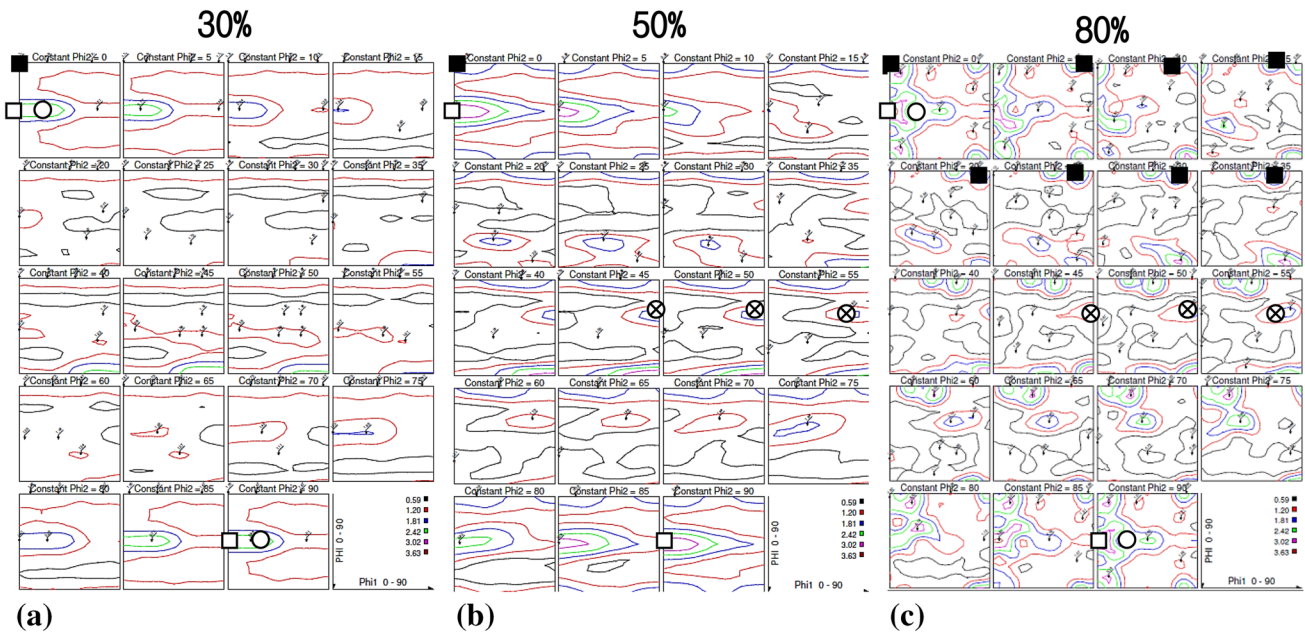

Fig. 5 ODF maps of samples deformed by different deformations. (a) 30%; (b) 50%; (c) 80%. Circled cross Copper component {112} ⟨111⟩; filled square Cubic component{001} ⟨100⟩; open square Goss component{011} ⟨100⟩; open circle Brass component {011} ⟨211⟩

Increasing the deformation temperature to 900 °C, coarse recrystallization grains appeared (Fig. 1f). When the deformation temperature was lower than 800 °C, the thermal activation

energy including the cumulative plastic strain energy was stored in deformation zones, such as the deformation bands and grain boundaries. As a result they could facilitate the recrys-
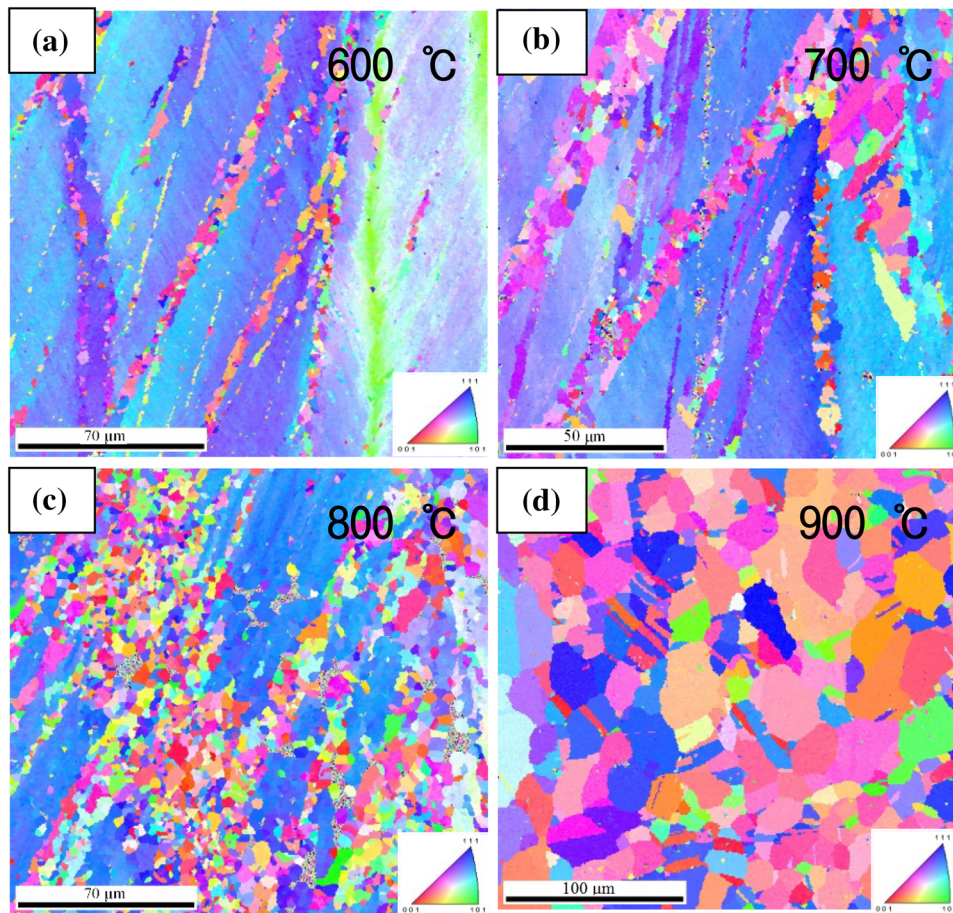
Fig. 6 EBSD micrographs of cold rolling specimens annealed at different temperatures for 1 h. (a) 600 °C; (b) 700 °C; (c) 800 °C; (d) 900 °C

tallization nucleation (Ref 24). When the deformation temperature was higher than 850 °C, dynamic recrystallization occurred completely.

Figure 2 shows EBSD images of the HCD samples deformed at different temperatures with a strain rate of 0.001 s^{-1}. The EBSD images show that sub-grains appeared in the HCD sample as it was hot deformed at 750 °C (Fig. 2a). When the sample was hot deformed at 800 °C (Fig. 2b), the sub-grains coarsened. As the HCD sample was hot deformed at 850 °C, sub-grains grew directly with the deformation temperature (Fig. 2c). Further increasing the deformation temperature to 900 °C, the sub-grains grew to tens of microns in size (Fig. 2d).

Figure 3 shows the pole figures of the HCD samples deformed at different temperatures. Cubic texture {001} ⟨100⟩ was formed in the HCD sample after being deformed at 750 °C (Fig. 3a). When the deformation temperature was 800 °C, Goss texture {011} ⟨100⟩ and rotated Cubic texture {001} ⟨110⟩ appeared (Fig. 3b). Further increasing the deformation temperature to 850 °C, Copper texture {112} ⟨111⟩, and Goss texture {011} ⟨100⟩ were formed (Fig. 3c). The pole figures of {100}, {101}, and {111} in Fig. 3d indicated that a great deal of recrystallization grains appeared as the sample was deformed at 900 °C. The types of texture components are mainly affected by the stacking fault energy of materials (Ref 25) and deformation mechanisms (Ref 26). In general, Copper texture usually appears in materials with medium or high stacking fault energy. As the specimens were deformed at a low temperature

of 750 °C, extensive cross-slip occurred, which led to the appearance of Cubic texture. With increasing deformation temperature, dynamic recrystallization occurred (Ref 27). The previous texture of {001} ⟨100⟩ was substituted by new grains with Goss texture. When the deformation temperature is 900 °C, the grains with Goss orientation were substituted by recrystallized grains with Copper texture.

3.2 Microstructure of Cold-Rolled Samples

Figure 4 shows the microstructure of the CRD specimens. Deformation bands appeared after the SSS specimens were cold rolled by 30% (Fig. 4b). The angles between the deformation bands and rolling direction were about 30° (Fig. 4b). Grains were elongated along the rolling direction with increased deformation. As the cold rolling deformation increased to 80%, processing fiber structure occurred in the CRD specimens (Fig. 4d). ODF maps of the CRD specimens are shown in Fig. 5. After the SSS sheets were cold rolled by 30% (Fig. 5a), Brass texture of {011} ⟨211⟩ was formed with a low density of 1.64. Increasing the deformation to 50% (Fig. 5b), Goss texture {011} ⟨100⟩ was formed with a density of 3.29. Further increasing the deformation to 80% (Fig. 5c), Goss, Cubic, and Brass textures were formed with density of 4.14, 3.8, and 2.41, respectively. Stacking fault energy plays an important role in the deformation of texture in face-centered cubic metals during plastic deformation (Ref 28). With increasing rolling deformation, more slip systems were activated; Brass, Goss, and Cubic
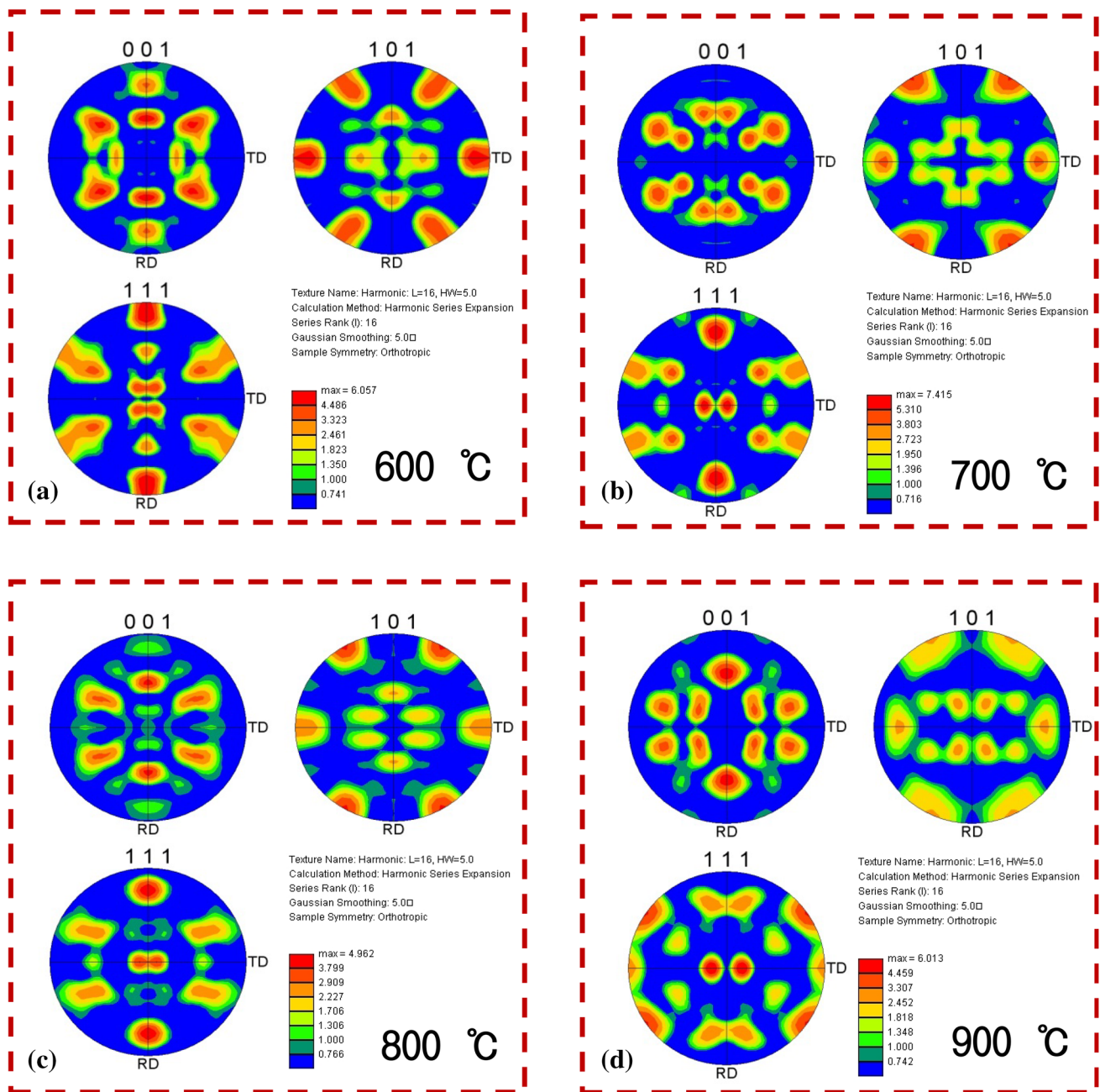
Fig. 7 Pole figure analysis of cold rolling alloys prior to annealed at different temperatures for 1 h. (a) 600 °C; (b) 700 °C; (c) 800 °C; (d) 900 °C

textures were formed in the elongated grains. These were a result of multitudinous cross-slips. Copper texture also appeared and grew in intensity for the cold-rolled grains with an increased number of deformation bands (Ref 29).

Figure 6 shows the EBSD micrographs of the CRD + AT specimens. After the specimens were annealed at 600 °C, the recrystallization preferentially nucleated in the deformation bands, grain boundaries, and triple junctions (Fig. 6a). After the specimens were annealed at 700 °C, volume fraction of static recrystallization grains increased (Fig. 6b). Increasing the annealing temperature to 800 °C, the volume fraction of recrystallization grains further increased (Fig. 6c). Some recrystallized grains grew after annealing at 900 °C. Equiaxed

recrystallization grains of about 30 μm were observed and a few annealing twins appeared (Fig. 6d).

Figure 7 shows the pole figures of the CRD + AT specimens. Goss, Cubic, and Brass textures were formed after annealing at 600 and 700 °C for 1 h (Fig. 7a and b). R texture {111} ⟨211⟩ was formed in the specimens after annealing at 800 °C for 1 h (Fig. 7c). After annealed at 900 °C for 1 h, recrystallization texture {001} ⟨100⟩ appeared in the specimens (Fig. 7d). During the cold rolling process, Goss texture appeared in elongated grains. The Goss texture was inherited after the samples were annealed at low temperatures (600 and 700 °C). However, after the annealing temperature was higher than 800 °C, recovery, dislocation movement and annihilation,

polygonization, and sub-crystal merging occurred in deformed grains. R and recrystallization textures became the mainly texture components (Ref 30).

Figure 8 shows the variation in hardness of the solution treated specimens followed by cold rolling by 50% and then
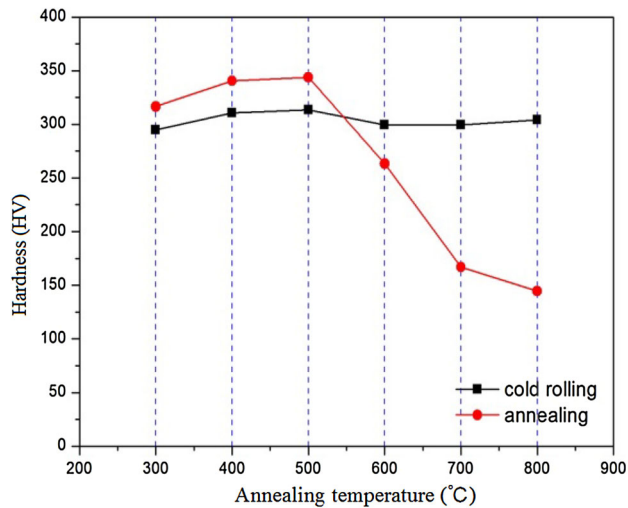
annealing at different temperatures for 1 h. As samples were annealed at low temperatures (300-500 °C), hardness increased. The higher the temperature, the more the hardness increased. Precipitation strengthening was the main reason for the hardness increase. After samples were annealed at elevated temperatures of 600-800 °C for 1 h, hardness decreased. The softening was due to static recrystallization and weak strengthening effect from coarse precipitates.

Figure 9 shows the TEM images of CRD + AT specimens. At a annealing temperature of 600 °C, nano-scale precipitation particles appeared inside the grains (Fig. 9a). When the annealing temperature increased beyond 700 °C, the density of dislocations decreased, recrystallization appeared, and precipitates still appeared in the specimens (Fig. 9b-d). Both recrystallizations and precipitation occurred during the annealing process (Ref 31, 32).

3.3 Microstructure of Multi-directional Forging (MDF) Samples

Figure 10 shows a series of distinctive optical micrographs of cryogenic temperature multi-directional forging (CTMDF) samples after different cycles. Fig. 10a shows one cycle's MDF sample ($\Delta \varepsilon_i = 0.6$), where the distinction between grain interiors and grain boundaries was obvious. It shows that deformation microstructure consisting of deformation bands in various directions which were clearly visible. A rough appearance developed in the coarse
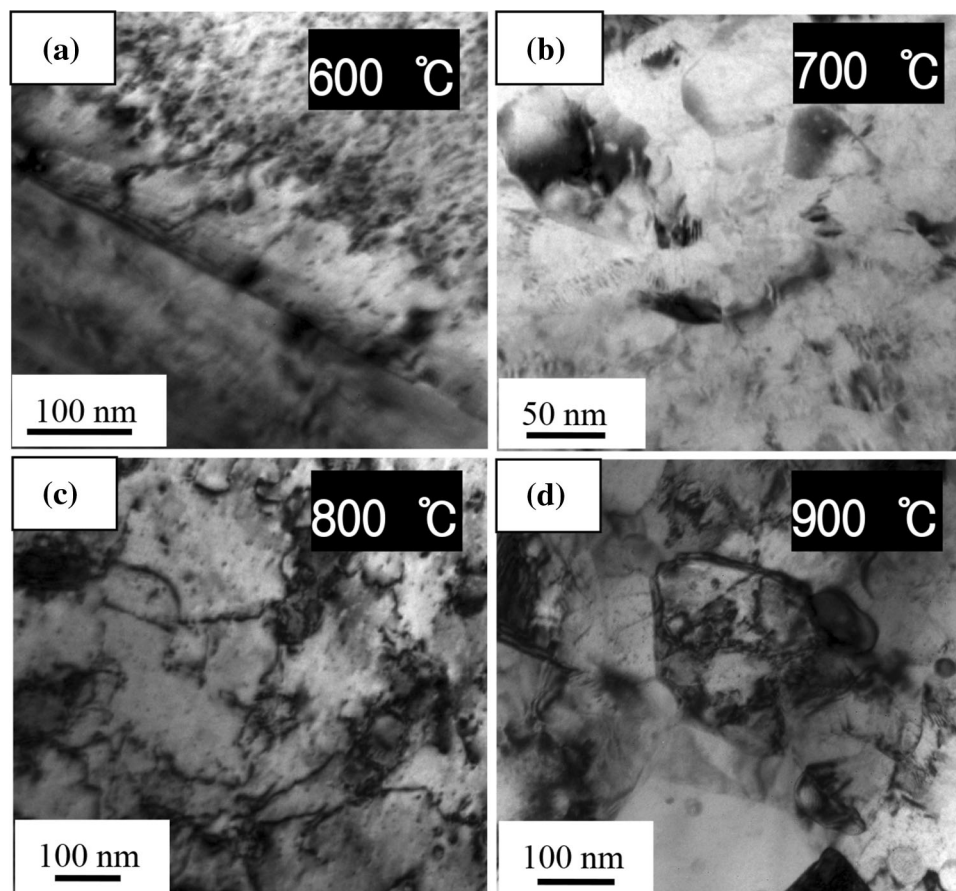

Fig. 9 Microstructure of cold-rolled specimens annealed at different temperatures for 1 h. (a) 600 °C; (b) 700 °C; (c) 800 °C; (d) 900 °C
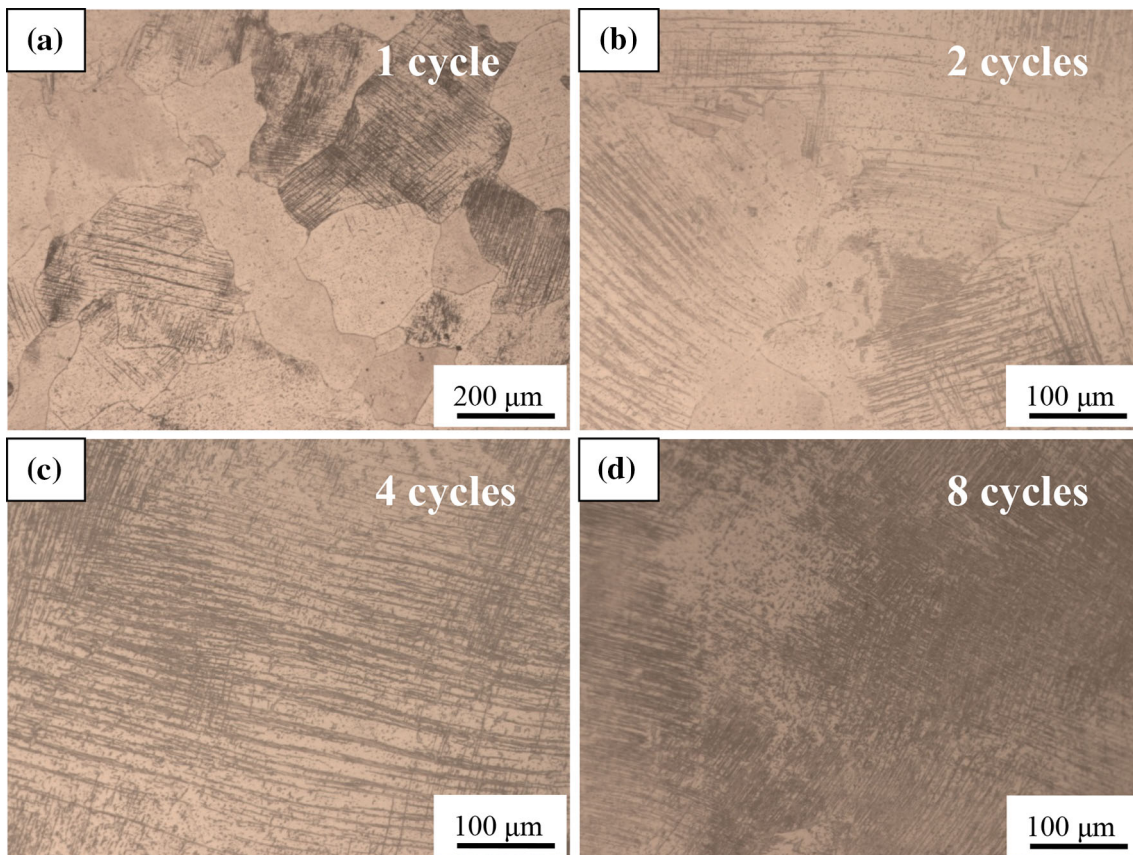
Fig. 10 Microstructure of specimens after multi-directional forging at cryogenic temperature by different cycles. (a) 1 cycle; (b) 2 cycles; (c) 4 cycles; (d) 8 cycles
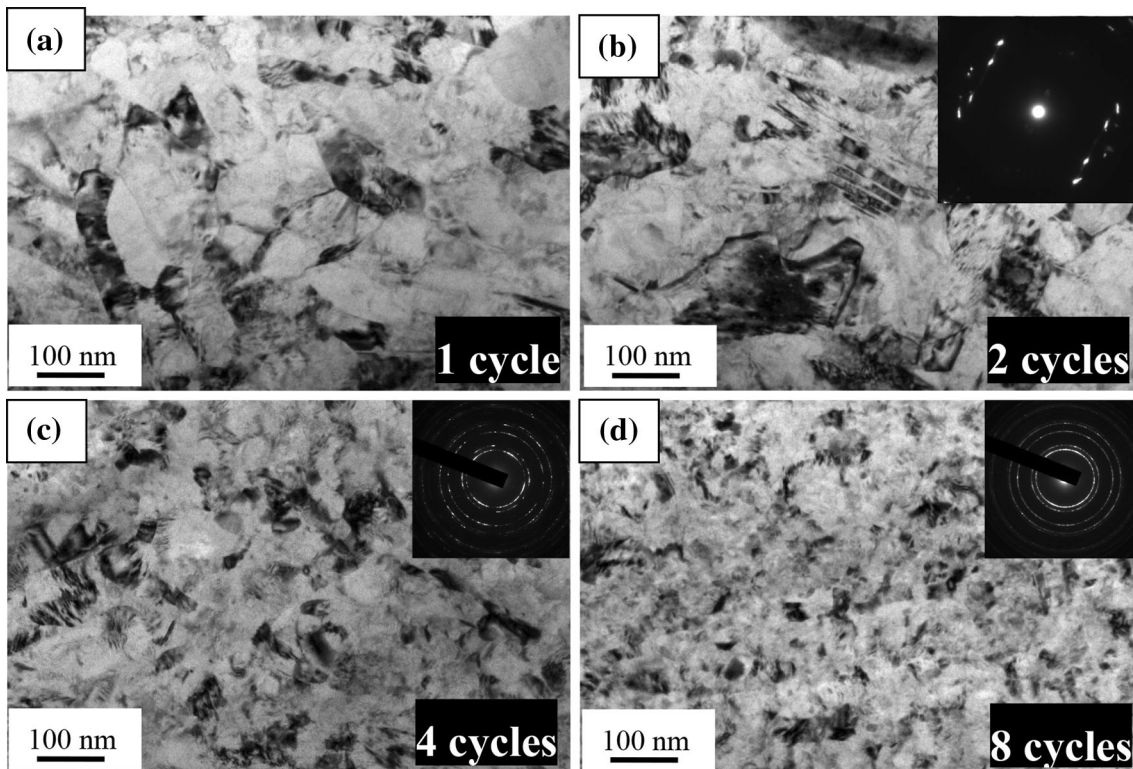

Fig. 11 TEM images of specimens after multi-directional forging at cryogenic temperature by different cycles. (a) 1 cycle; (b) 2 cycles; (c) 4 cycles; (d) 8 cycles

grained samples owing to the increased density of deformation bands (Fig. 10a). With increased number of the cycles, the coarse grains were broken into fine sub-grains (Fig. 10b-d).

Figure 11 shows the TEM micrographs corresponding to CTMDF up to 8 cycles. Formations of sub-grains with an average size of 150 nm along with the presence of high density of dislocations were revealed in the samples after 1 cycle (Fig. 11a). The dislocation density increased with increasing strain and suppression of dynamic crystallization lead to formation of fine sub-grains. The SADP in Fig. 11b shows deformation twins formed in the samples under multi-directional forging at cryogenic temperature for 2 cycles. The sub-grains size was decreased to 100 nm. With an increasing number of cycles, the sub-grain size was reduced to an average size of 60 nm in Fig. 11c (4 cycles) and 50 nm in Fig. 11d (8 cycles). The SADP in Fig. 11c and d revealed that the sub-grains were refined and maintained crystal orientation. With increased number of cycles, the average size of sub-grains was reduced.

Hardness changes between the RTMDF and CTMDF samples were investigated and the results are summarized in Fig. 12. It can be seen in Fig. 12 that the hardness increased proportionally with the cumulative strain in both RTMDF and CTMDF samples. The hardness increased greatly during several early cycles, as the samples were RTMDF-ed and CTMDF-ed through 3 cycles, as a result their hardness values increased by 49.2% and 64.9%, respectively. And after being MDF-ed by 8 cycles (cumulative strain of 4.8), their hardness values increased by 58.3 and 73.0%. The high increases in hardness at low strain are due to the work hardening as opposed to those at higher cumulative strain. The hardness further increased because of work hardening and grain refinement strengthening. This was attributed to the formation of equiaxed sub-grain structures and the presence of high dislocation density. In the present study, samples were MDF-ed up to 8 cycles without any cracks. The grain size of a Cu-2.5Ni-0.6Si alloy processed by equal-channel angular pressing at 423 K was refined to an average value of about 0.9 μm (Ref 33). High-pressure torsion at room temperature with an imposed pressure for 5 turns reduced the grain size of the Cu-2.9Ni-0.6 Si alloy to 150 nm (Ref 34). Combination of swaging and subsequent optimized precipitation hardening refined the grain
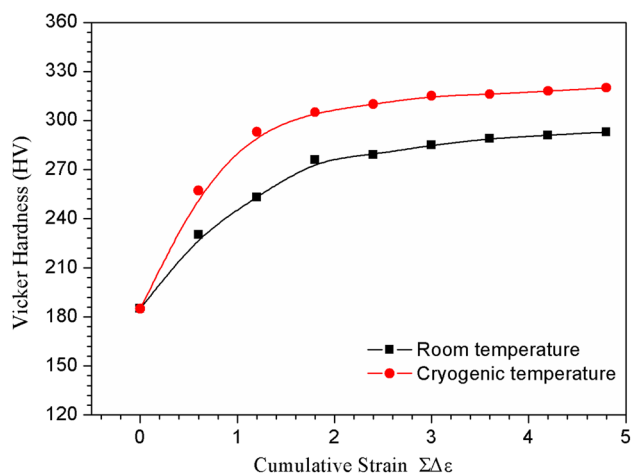
size of the Cu-3Ni-1Si-0.1Mg alloy in the range of 0.2-2 μm. Following aging at 527 K for 200 h, the ultimate tensile strength is possibly higher than 1000 MPa (Ref 35). For the studied Cu-Ni-Si alloy, multi-directional forging at cryogenic temperature is an effective way to refine the microstructure and to enhance the hardness.

4. Conclusions

(1) Dynamic recrystallization appeared to preferentially abut deformation bands after the samples were hot-compressive deformed at 750 °C. At deformation temperature of 850 °C, dynamic recrystallization grain size was 10 μm. Furthermore, grain size grew to 30 μm at deformation temperature of 900 °C. With the deformation temperature increasing from 750 to 900 °C, elongated grains with the Cubic texture {001} ⟨100⟩ were substituted by the fully recrystallized grains with a Copper texture {112} ⟨111⟩.

(2) For the CRD + AT samples, Goss, Cubic, and Brass textures were formed after the cold-rolled samples were annealed at 600 and 700 °C. R texture were formed as the cold-rolled samples were annealed at 800 °C. Further increasing the annealing temperature to 900 °C, led to the formation of recrystallization texture {001} ⟨100⟩.

(3) For the samples undergone multi-directional forging at cryogenic temperature, sub-grain/grains size decreased with the MDF-ed cycles. Compared with those samples deformed at room temperature, the hardness of the samples that underwent deformed at cryogenic temperature was greater. The hardness was further improved as a result of work hardening and grain refinement strengthening, which are attributed to the formation of equiaxed sub-grain structures and the presence of high dislocation density.

Fig. 12 Change of Vickers hardness at room and cryogenic temperature of multi-directional forging samples with different cycles

References

1. Q.Y. Dong, L.N. Shen, F. Cao, Y.L. Jia, K.J. Liao, and M.P. Wang, Effect of Thermomechanical Processing on the Microstructure and Properties of a Cu-Fe-P Alloy, *J. Mater. Eng. Perform.*, 2015, **24**(4), p 1531–1539

2. H.C. Chen, G. Bi, M.L.S. Nai, and J. Wei, Enhanced Welding Efficiency in Laser Welding of Highly Reflective Pure Copper, *J. Mater. Process. Technol.*, 2015, **216**, p 287–293

3. A.Y. Khereddine, F.H. Larbi, M. Kawasaki, T. Baudin, D. Bradai, and T.G. Langdon, An Examination of Microstructural Evolution in a Cu-Ni-Si Alloy Processed by HPT and ECAP, *Mater. Sci. Eng. A*, 2013, **576**, p 149–155

4. I. Shakhova, Z. Yanushkevich, I. Fedorova, A. Belyakov, and R. Kaibyshev, Grain Refinement in a Cu-Cr-Zr Alloy During Multidirectional Forging, *Mater. Sci. Eng. A*, 2014, **606**, p 380–389

5. H. Tsubakino, R. Nozato, and A. Yamamoto, Precipitation Sequence for Simultaneous Continuous and Discontinuous Modes in Cu-Be Binary Alloys, *Mater. Sci. Technol.*, 1993, **9**(4), p 288–294

6. B. Djurić, M. Jovanović, and D.J. Drobnjak, A Study of Precipitation in Cu-Be Alloys, *Metallography*, 1980, **13**, p 235–247

7. W.S. Jeon, C.C. Shur, J.G. Kim, S.Z. Han, and Y.S. Kim, Effect of Cr on the Corrosion Resistance of Cu-6Ni-4Sn Alloys, *J. Alloys Compd.*, 2008, **455**, p 358–363

8. F.L. Wang, Y.P. Li, K. Wakoh, Y. Koizumi, and A. Chiba, Cu-Ti-C Alloy with High Strength and High Electrical Conductivity Prepared by Two-Step Ball-Milling Processes, *Mater. Des.*, 2014, **61**, p 70–74

9. L.N. Shen, Z. Li, Z.M. Zhang, Q.Y. Dong, Z. Xiao, Q. Lei, and W.T. Qiu, Effects of Silicon and Thermo-mechanical Process on Microstructure and Properties of Cu-10Ni-3Al-0.8Si Alloy, *Mater. Des.*, 2014, **62**, p 265–270

10. W.H. Sun, H.H. Xu, S.H. Liu, Y. Du, Z.H. Yuan, and B.Y. Huang, Phase Equilibria of the Cu-Ni-Si System at 700 °C, *J. Alloys Compd.*, 2011, **509**(41), p 9776–9781

11. S.A. Lockyer and F.W. Noble, Precipitate Structure in a Cu-Ni-Si Alloy, *J. Mater. Sci.*, 1994, **29**(1), p 218–226

12. Q. Lei, Z. Li, J. Wang, J.M. Xie, X. Chen, S. Li, Y. Gao, and L. Li, Hot Working Behavior of a Super High Strength Cu-Ni-Si Alloy, *Mater. Des.*, 2013, **51**, p 1104–1109

13. X.J. Liu, S.L. Xiang, S.Y. Yang, R.P. Shi, and C.P. Wang, Experimental Investigation of Phase Equilibria in the Cu-Ni-Si Ternary System, *J. Alloys Compd.*, 2013, **578**, p 439–447

14. H. Azzeddine, B. Mehdi, L. Hennet, D. Thiaudière, B. Alili, M. Kawasaki, D. Bradai, and T.G. Langdon, An In Situ Synchrotron X-Ray Diffraction Study of Precipitation Kinetics in a Severely Deformed Cu-Ni-Si Alloy, *Mater. Sci. Eng. A*, 2014, **597**, p 288–294

15. C. Watanabe and R. Monzen, Coarsening of δ-Ni₂Si Precipitates in a Cu-Ni-Si Alloy, *J. Mater. Sci.*, 2011, **46**(12), p 4327–4335

16. Z.Y. Pan, M.P. Wang, Z. Li, C.P. Deng, S.H. Li, and Y.L. Jia, Progress of Study of Super-High Strength Cu-Ni-Si Alloy, *Heat Treat. Met.*, 2007, **7**, p 55–59

17. Z. Li, Z.Y. Pan, Y.Y. Zhao, Z. Xiao, and M.P. Wang, Microstructure and Properties of High Conductivity, Super High Strength Cu-8.0Ni-1.8Si-0.6Sn-0.15Mg Alloy, *J. Mater. Res.*, 2009, **24**, p 2123–2129

18. Q. Lei, Z. Li, M.P. Wang, L. Zhang, Z. Xiao, and Y.L. Jia, The Evolution of Microstructure in Cu-8.0 Ni-1.8 Si-0.15 Mg Alloy During Aging, *Mater. Sci. Eng. A*, 2010, **527**, p 6728–6733

19. J.Y. Cheng, B.B. Tang, F.X. Yu, and B. Shen, Evaluation of Nanoscaled Precipitates in a Cu-Ni-Si-Cr Alloy During Aging, *J. Alloys Compd.*, 2014, **614**, p 189–195

20. A.Y. Khereddine, F.H. Larbi, H. Azzeddine, T. Baudin, F. Brisset, A.L. Helbert, M.H. Mathon, M. Kawasaki, D. Bradai, and T.G. Langdon, Microstructures and Textures of a Cu-Ni-Si Alloy Processed by High-Pressure Torsion, *J. Alloys Compd.*, 2013, **574**, p 361–367

21. Q. Lei, Z. Li, C. Dai, J. Wang, X. Chen, J.M. Xie, W.W. Yang, and D.L. Chen, Effect of Aluminum on Microstructure and Property of Cu-Ni-Si Alloys, *Mater. Sci. Eng. A*, 2013, **572**, p 65–74

22. Q. Lei, Z. Li, T. Xiao, Y. Pang, Z.Q. Xiang, W.T. Qiu, and Z. Xiao, A New Ultrahigh Strength Cu-Ni-Si Alloy, *Intermetallics*, 2013, **42**, p 77–84

23. T. Konkova, S. Mironov, A. Korznikov, and S.L. Semiatin, Microstructural Response of Pure Copper to Cryogenic Rolling, *Acta Mater.*, 2010, **58**, p 5262–5273

24. Y.P. Lü, D.A. Molodov, and G. Gottstein, Recrystallization Kinetics and Microstructure Evolution During Annealing of a Cold-Rolled Fe-Mn-C Alloy, *Acta Mater.*, 2011, **59**, p 3229–3243

25. J.J. Sidor and L.A.I. Kestens, Analytical Description of Rolling Textures in Face-Centred- Cubic Metals, *Scr. Mater.*, 2013, **68**(5), p 273–276

26. N. Jia, Z.H. Nie, Y. Ren, R.L. Peng, Y.D. Wang, and X. Zhao, Formation of Deformation Textures in Face-Centered-Cubic Materials Studied by In-Situ High-Energy X-Ray Diffraction and Self-Consistent Model, *Metall. Mater. Trans. A*, 2010, **41**(5), p 1246–1254

27. Y. Huang and P.B. Prangnell, The Effect of Cryogenic Temperature and Change in Deformation Mode on the Limiting Grain Size in a Severely Deformed Dilute Aluminium Alloy, *Acta Mater.*, 2008, **56**(7), p 1619–1632

28. R.E. Smallman and D. Green, The Dependence of Rolling Texture on Stacking Fault Energy, *Acta Metall.*, 1964, **12**(2), p 145–154

29. S.H. Kim, S.Z. Han, C.J. Kim, I.Y. Hwang, and F.X. Yin, Evolution of Rolling Textures of Cold Rolled Copper Foils, *Mater. Trans.*, 2009, **50**(3), p 537–543

30. I.A. Yakubtsov, A. Ariapour, and D.D. Perovic, Effect of Nitrogen on Stacking Fault Energy of F.C.C. Iron-Based Alloys, *Acta Mater.*, 1999, **47**(4), p 1271–1279

31. Q. Lei, Z. Li, A.Y. Zhu, W.T. Qiu, and S.Q. Liang, The Transformation Behavior of Cu-8.0Ni-1.8Si-0.6Sn-0.15Mg Alloy During Isothermal Heat Treatment, *Mater. Charact.*, 2011, **62**, p 904–911

32. Q. Lei, Z. Li, J. Wang, S. Li, L. Zhang, and Q.Y. Dong, High-Temperature Deformation Behavior of Cu-6.0Ni-1.0Si-0.5Al-0.15 Mg-0.1Cr Alloy, *J. Mater. Sci.*, 2012, **47**, p 6034–6042

33. F.H. Larbi, H. Azzeddine, T. Baudin, M.H. Mathon, F. Brisset, A.L. Helbert, M. Kawasaki, D. Bradai, and T.G. Langdon, Microstructure and Texture Evolution in a Cu-Ni-Si alloy Processed by Equal-Channel Angular Pressing, *J. Alloys Compd.*, 2015, **638**(25), p 88–94

34. H. Matsunaga, Z. Horita, K. Imamura, T. Kiss, and X. Sauvage, Aging Behavior of Cu-Ni-Si Alloy Processed by High-Pressure Torsion, *Mater. Sci. Form.*, 2011, **667–669**, p 307–312

35. I. Altenberger, H.A. Kuhn, M. Gholami, M. Mhaede, and L. Wangner, Ultrafine-Grained Precipitation Hardened Copper Alloy by Swaging or Accumulative Roll Bonding, *Metals*, 2015, **5**, p 763–766